Chapter 21
Crystal Lattice Defects as Natural Light Emitting Nanostructures in Semiconductors

Oleg Vyvenko and Anton Bondarenko

Abstract The review summarizes previous and very recent data on the luminescent properties of natural low-dimensional nanostructures in tetrahedrally coordinated semiconductors which are two particular types of extended crystal lattice defects: stacking faults (SF) and dislocations. Experimental data obtained in diamond-like, zink-blend and wurtzite lattice structures revealed intrinsic luminescence bands with the specific for given material properties for both types of the defects. The data are discussed in the framework of suggested theoretical models and non-solved issues of the interpretation are underlined. An unexpected intrinsic luminescence of quantum barriers formed by SF in sphalerite crystals caused by its dipole moment due to spontaneous polarization in wurtzite phase SF of the width even as narrow as dislocation dissociation width as well as the presence of quantum well formed by SF in wurtzite type crystals are suggested to be included for the revision of the previous interpretation of the dislocation-related luminescence mechanisms. The possibility of usage of the extended defects as active elements of light-emitting devices is considered.

21.1 Introduction

Low-dimensional structures such as quantum wells (QW), quantum wires (QWR), and quantum dots (QD) are the basis of modern semiconductor photonics. Of particular interest are zero-dimensional (0D) and one-dimensional (1D) systems due to singularities in their N (E) state density, which leads to an enhancement of probability of carrier recombination and, consequently, of the efficiency of light-emitting devices (LED) and a lowering of the lasing threshold. In addition, one-dimensional systems are also interesting from the point of view of the phenomenon of quasi-one-dimensional conductivity, which can find application in the development of future

O. Vyvenko (✉) · A. Bondarenko
Institute of Physics, St. Petersburg State University, Uljanovskaja 1, 198504 St. Petersburg, Petrodvoretz, Russia
e-mail: vyvenko@nano.spbu.ru

A. Bondarenko
e-mail: anton.bondarenko@spbu.ru

© Springer Nature Switzerland AG 2019

K. Yamanouchi et al. (eds.), *Progress in Photon Science*, Springer Series in Chemical Physics 119, https://doi.org/10.1007/978-3-030-05974-3_21

generations of high-performance field-effect transistors. Today, low-dimensional structures are manufactured mainly using epitaxial growth methods, which make it possible to obtain very efficient light-emitting semiconductor devices based on QWs and QDs [1, 2]. The technology of growth of such structures is based on layer-by-layer growth and self-assembly for QDs has reached the industrial level. The fabrication of quasi-1D structures needs to include additional technological steps and is far more complicated. Several attempts to develop the methods of the growth of quasi-1D structures were reported previously but no one brought their desirable quality. The etching of quantum wires through a lithographic pattern from grown QW suffers from the heterogeneity of the chemical composition over the QW area, which may not be noticeable when working with a 2D system, but it critically affects the properties of QWR. The epitaxial overgrowing of pre-prepared grooves, using the segregation of atoms of some elements with higher mobility, such as In and Al, at sites of local minima of potential energy [3] is actively developing but a rather low density of the structures were obtained so far. The T-shaped QWRs obtained by overgrowth on the cleavage of a structure with a QW with another QW [4] have demonstrated good optical properties in laboratory studies but this approach is very inefficient economically for industrial use. Finally, the direct epitaxial growth of nanowires (NW) [5] enables to grow their high density array with well controlled chemical composition but a variation of NW diameters commonly occurs and there is a lack of technology to reliably manipulate grown NWs for the device manufacturing.

In this review, an alternative approach to creating low-dimensional structures is considered, based on the use of intrinsic extended defects in crystalline semiconductors: dislocations and stacking faults (SF). The main advantage of this approach is the absence uncontrolled temporal and spatial variation of chemical composition which are unavoidable by the epitaxial growth of heterostructures. The dislocation line inside the crystal breaks the translational symmetry of the crystal near its core forming a particular atomic configuration. In the most tetrahedrally coordinated semiconductors the core consists of a composition of packing defect ribbon, staking fault (SF), and two bounded partial dislocations (PD) that has been experimentally established by high resolution transmission electron microscopy (HR-TEM) [6] and that coincides well with predicted by the density functional theory (DFT) methods [7]. Translational symmetry and the long-acting attracting potential of the field of mechanical stresses are the reason for the formation of 1D bands of allowed energy states, which turns a dislocation into a 1D QWR natural for any crystal [8]. The properties of dislocations in semiconductors, such as the increased mobility of carriers [9] and dislocation luminescence [10, 11], which are most demanded from the point of view of applications, are due precisely to the presence of these 1D bands. Besides, the dislocations can form nodes at the points of intersection of dislocations that can be considered as 0D quantum dots.

21.2 One- and Two-Dimensional Defects in Semiconductors with Face Centered Cubic (FCC) and Hexagonal Closest Packed (HCP) Lattices

21.2.1 Structure and Energetics

Most semiconductors with cubic crystal system have either diamond cubic structure for elemental semiconductors (group IV semiconductors) or zinc-blende (ZB), or sphalerite, crystal structure for compound semiconductors (II–VI, III–V semiconductors) [12]. Both diamond and ZB crystal structures follow face-centered cubic (fcc) Bravais lattice with two atoms in its basis set (Fig. 21.1 a, b) at (0, 0, 0) and (¼, ¼, ¼). In diamond structure basis set atoms are of the same kind whereas in ZB they differ, which adds ionic component to covalent bonds. Each atom in diamond and ZB structures is four-fold coordinated by its neighbors forming a tetrahedra, which orientation makes two atoms in basis set distinguishable and opposite directions along <111> not equivalent, denying inversion symmetry operation.

Dislocations are defined as the line bounded the region of non-complete shear displacement of one part of the crystal with respect to another. Main characteristics of a dislocation are its direction and the direction and the value of the displacement called as Burgers vector. Allowed Burgers vectors for perfect dislocation in diamond

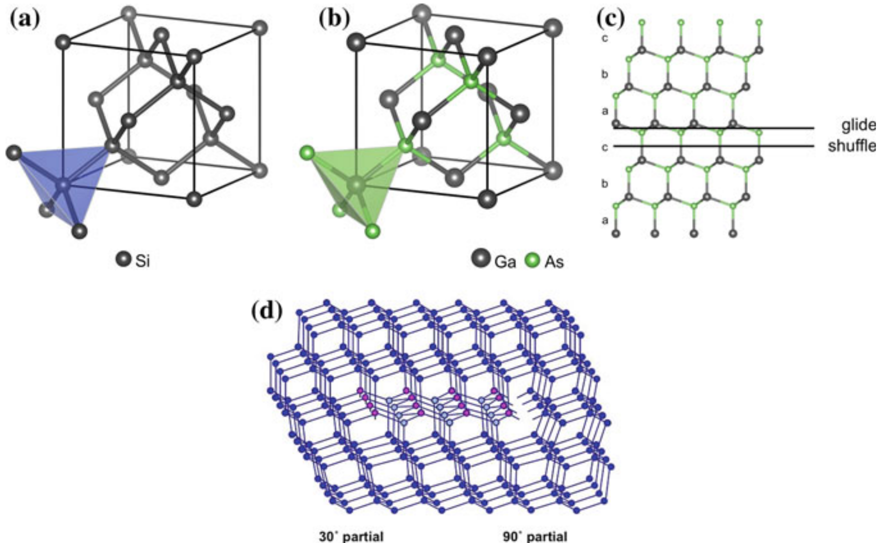

Fig. 21.1 Ball and stick model of diamond-like structure (**a**) and of zinc blende crystal structure (**b**). Tetrahedra show four-fold symmetry of bonds. Zinc blende stacking (**c**), atomic structure of the core of dissociated 60° dislocation in diamond [13] consisting of SF ribbon and bounded partials (**d**)

and ZB structures are ½<110> the same as for fcc lattice according to Frank's energy criterion [14]. For dislocations with Burgers vector ½<110> there are three possible slip planes: (100), (110), and (111). However, only the (111) slip plane was observed experimentally in fcc lattice. In (111) slip plane only two perfect dislocations are possible. Screw dislocation, and 60°-dislocation [15].

From the other hand, fcc lattice can be viewed as a stack of close-packed atomic layers in (111) planes. Atoms of consequent layers occupy one of three different sets of positions labeled a, b, and c. The perfect fcc lattice has stacking sequence of either abcabc or cbacba. The presence of additional layer in diamond and ZB stacking allows for two possible sets of slip planes. One is the glide set between close-spaced layers, the other is the shuffle set between the couples of the close-spaced ones. Transmission electron microscopy (TEM) experiments using weak beam technique [16] showed, that in diamond-like structures dislocations belong mostly to glide set and almost always are dissociated into partial dislocations bounding stacking fault (SF) ribbon (Fig. 21.1d) [17, 18].

SF is 2D defect, which arises when perfect lattice abcabc stacking is disturbed by either removal (intrinsic SF) or insertion (extrinsic SF) of a layer. In fcc lattice one may construct one intrinsic SF abcbca and one extrinsic SF abcbab (Fig. 21.2) [19]. If SF is surrounded by a perfect crystal from all sides it must be bound by 30° and 90° partial dislocations (left and right in Fig. 21.1d) [15, 17–19].

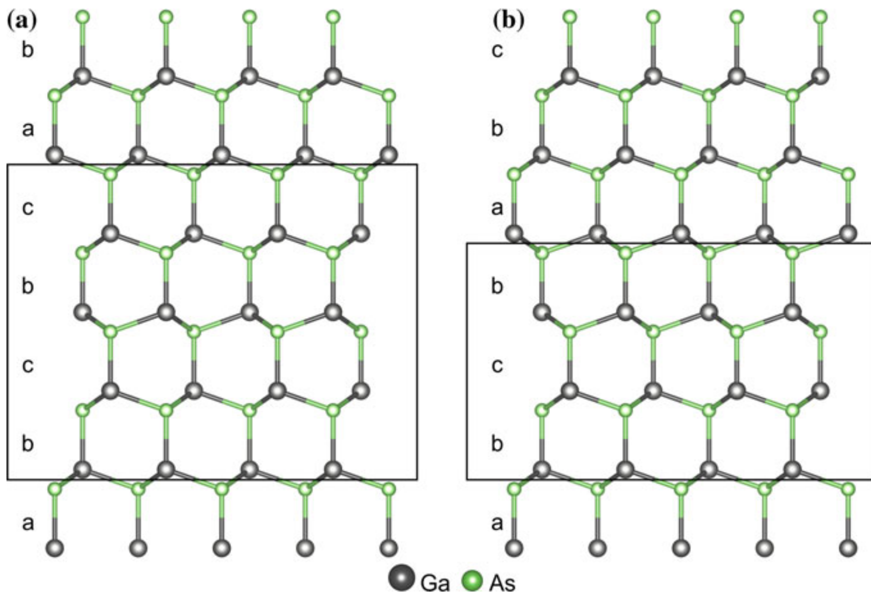

Fig. 21.2 Ball and stick model of GaAs zinc blende structure with intrinsic (**a**) and extrinsic (**b**) stacking faults. Projection along [110], vertical axis is [111]. Rectangle frames outline hexagonal stacking patterns bcbc

SF in diamond or ZB crystal structure can be considered as an inclusion of very thin hexagonal wurtzite phase bcbc-stacking layer (Fig. 21.2).

The wurtzite crystal structure (WZ) is a hexagonal type lattice containing atoms of two different elements. Two parameters a and c are only needed to completely describe WZ-type lattice, where a is side of the base of vertical prism of the primitive unite cell and c is the height of the prism. Atoms of each type form two hexagonal close-packed (HCP) sublattices positioned directly one upon another and separated in ideal WZ structure along the [0001] c-axis by 3/8c. As well as in ZB crystal structure each atom in WZ lattice is tetrahedrally coordinated, however, unlike in cubic ZB lattice the bonds do not have to be of the same length to keep the lattice symmetry. Actually, some binary semiconductors (almost all III-nitrides, except BN) always crystallize in WZ structure because of high difference in size of the atoms, which leads to formation of short bonds with large ionicity between atoms of close spaced layers in basal planes and longer bonds along vertical c-axis of the primitive unit cell [20, 21]. This makes c-axis a singular polar axis and is responsible for piezoelectricity known for many semiconductors with WZ crystal structure. Large ionic component also plays crucial role in performance of devices based on WZ-structure semiconductors due to emergence of large internal electric fields caused by spontaneous polarization [22].

In perfect WZ crystal structure stacking sequence along the c-axis has abab pattern. As it was first analyzed by Frank and Nicholas in [19] HCP lattice may have three types of stacking faults shown in Fig. 21.3. These are two intrinsic stacking faults I_1 and I_2, and extrinsic stacking fault E, which can be viewed as the inclusions of ZB-layers with abcabc stacking pattern. Each SF independently on its type must be bound by partial dislocations in (0001) plane unless it is coming out to the surface of the crystal.

In WZ-type lattice the shortest translation vector is primitive unit cell vector a 1/3 [–12–10], which allows four perfect dislocations in the (0001) plane [23]. These are 0° screw (a-screw) dislocation along [–12–10], 90° edge dislocation along [–1010], 60° dislocation along [–2110], and 30° dislocation along [–1100]. Each of these dislocations can dissociate into partials by the reactions described in [24]. Besides there is perfect, non-dissociated, prismatic 90° edge dislocation along [0001].

21.2.2 Dislocations as Quantum Conducting Wires

The dislocation electronic bound states were studied both experimentally and theoretically because they determine electrical activity of dislocations. Density functional theory (DFT) calculations [25, 26] predict that the cores of dislocations are heavily reconstructed, which lead to absence of any dangling bonds shown in Fig. 21.1d. This explains why DFT calculations do not predict any dislocation-related deep levels in the band gap for many materials studied, but only shallow bound states near to the band edges. These shallow states originate from long-range elastic strain fields, self-consistently accounted for by DFT methods. However, DFT methods are

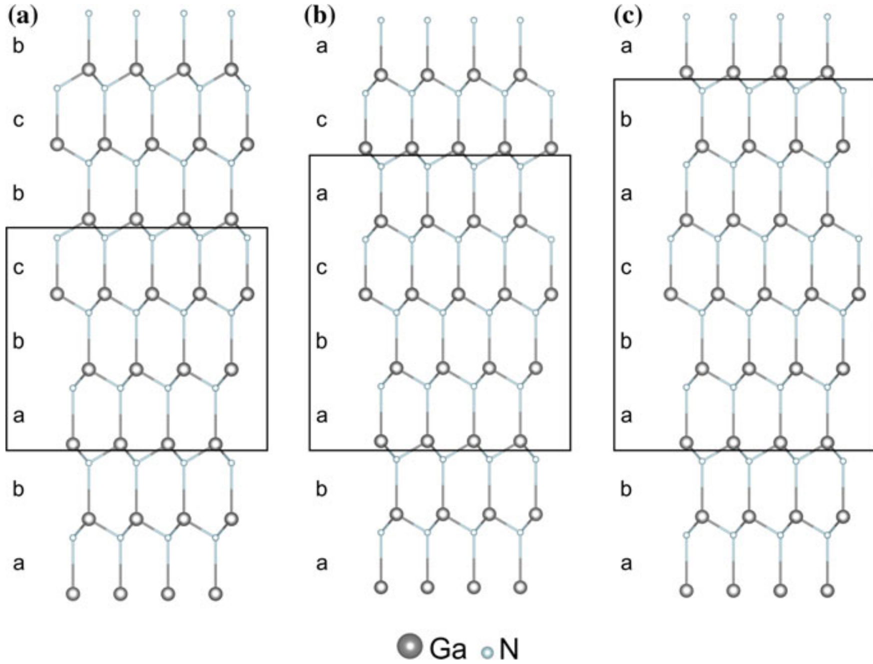

Fig. 21.3 Possible types of stacking faults in wurtzite crystal structure. Intrinsic stacking faults I_1 (**a**) and I_2 (**b**), and extrinsic stacking fault E. Projection along [10–10] vertical axis along wurtzite c-axis [0001]

only precise in calculation of total energy of the supercell and cannot provide exact energy positions for shallow bound levels in the band gap. To overcome this limitation some efforts were undertaken to calculate the shallow bounds states of dislocation deformation potential using the envelope function technique in the effective mass approximation [8, 27, 28]. Using this approach it was shown [8] that for many diamond and ZB semiconductors the deformation potential is responsible for formation of 1D bands for both electrons and holes with binding energy of about 50–80 meV.

1D dislocation bands must be responsible for enhanced conductivity of dislocations observed in many experiments [9, 29–32]. In CdS 1D-like enhanced conductivity of screw dislocations was detected by direct current measurement [29]. In Ge 1D conductivity of 60° dislocations was well established by both DC and AC measurements [30, 31]. In Si enhanced conductivity of dislocations was observed only after the hydrogenation procedure [30], which is known to passivate deep levels [33, 34]. However, in GaAs no evidence of dislocation conductivity was found for both screw and 60° dislocations [31]. Enhanced conductivity of threading dislocations in GaN was observed by means of scanning spread resistance measurement [32].

The development of direct wafer bonding technique [35] allowed for the experimental investigation of charge carrier transport mechanisms of individual dislocation in Si by preparation of tunnel field effect transistor with defined number and type of dislocations [9]. It was demonstrated that individual dislocations form additional tunneling paths result in formation of only one or a few bands in the band gap.

21.2.3 Stacking Faults as Quantum Wells

Electronic states of a SF can originate from bounding partial dislocations or from the fact, that stacking fault is actually a thin layer of another crystalline phase of the same material. Theoretical investigations [36] have shown that in Si stacking fault gives level with energy of about Ev + 0.1 eV, which depend on SF width. Later calculations [37] showed that this energy level does not depend on the structure of bounding dislocation but on the overlap of the wave functions of SF states, which increase when partials are close together. The energy of SF states in Si was predicted in the range Ev + 0.075 eV for infinite SF width and Ev + 0.21 eV for SF ribbon width of 2.3 nm.

In compound semiconductors ZB and WZ phases possess different band gaps. In all known cases band gap of WZ exceeds that of ZB as it is summarized in Table 21.1.

As the result SF in WZ phase being an insertion of ZB one forms QW while SF in ZB forms a barrier at least for one type of charged carriers.

Exact alignment of band structure is unknown in many cases. A good example is WZ GaN where luminescence measurement on SF-rich samples revealed new bands which allowed for development of theoretical model of intrinsic SF in GaN as a compressed by dislocation deformation potential cubic phase inclusion [39]. The model predicts a quantum well for electrons $\Delta Ec = 0.122$ eV and a barrier for holes $\Delta Ev = 0.062$ eV for I_2-type SF. Later, this model was enhanced in [22, 40] by accounting for the electric field of spontaneous polarization of WZ GaN, which allowed from one hand to explain the peculiarities of SF-luminescence and from the other hand to estimate spontaneous polarization in GaN (for more details see Sect. 21.6).

Table 21.1 Difference of the band gap energy in eV between WZ and ZB crystal structure for common binary semiconductors (see [38] and references therein)

	WZ	ZB	ΔE (WZ − ZB)
GaN	3.4	3.2	0.2
CdS	2.5	2.37	0.13
ZnS	3.77	3.68	0.09
SiC-2H-6H	2.9–3.3	2.3	0.6–1.0
ZnSe	2.8	2.7	0.1
GaAs	1.46	1.42	0.035–0.055

21.3 Dislocation-Related Luminescence in Ge and Si

Historically, dislocation related luminescence (DRL) was found firstly in Ge [41] in 1957 and nearly 20 years later in Si [10]. Afterwards, a lot of the papers were published until the very recent time. More detailed reviews about the state-of-the-art status of experimental data and of the mechanism understanding can be found elsewhere [42–46].

The most results on DRL in Si were obtained on the samples with dislocations introduced by plastic deformation though similar data were reported for misfit dislocations at heterointerfaces [47], and more recently, on dislocation networks produced by silicon wafer bonding [48, 49].

It was discovered that the DRL spectra (4a) consisted of a set of narrow lines in both materials. In silicon four main lines denoted as D1–D4 in the ranges 0.8–1.0 eV were divided in two groups D1–D2 and D3–D4 with well distinguished properties [51]. D3–D4 lines could be observed only at very low temperature while D1–D2 remained rather intensive even at room temperature. Cathodoluminescence (CL) with a high spatial resolution revealed that D3–D4 stemmed from dislocation lines whereas D1 in the areas between them [47]. Besides, a strong enhancement of D1 DRL due to light contamination with transition metals was established [47, 52]. The thermal stability of D1 DRL gave the hope to use it for silicon based light emitter compatible with CMOS technology and numerous investigations were performed (for recent review see [45]) and examples of D1 DRL based device fabrication were described [33, 53]. Nevertheless, an exact knowledge about the origin and mechanism of D1 DRL is still absent.

Finally, it was established that that D3 line is the phonon replica of D4 and that the latter exhibited a fine structure that can appear by varying the deformation conditions, and disappear by the annealing at sufficiently high temperature [50, 54]. It is significant that the spectral positions of the observed D4 DRL fine structure components practically never changed (Fig. 21.4b). The individual lines were numbered with integers [50] and it was postulated that radiative transitions of pairs of point centers participate in the processes, and the distance between the centers in such pairs was proposed to be defined by the SF ribbon width in the core of dissociated dislocations being the discrete parameter influencing the spectral frequency of the radiation.

The thorough investigations of the dislocation photoluminescence in Ge crystals in [44, 55] led to a more detailed picture of the origin of the spectral series (see Fig. 21.5). The importance of the dissociation of dislocations into partial dislocations (or partials) separated by stacking fault with a set of discrete widths was revealed similarly to the DRL in silicon. Actual direct experimental evidence of this was obtained in [55] by applying a specially oriented additional load, which caused either an increase or a decrease in the dissociation of the dislocations producing mostly short-wavelength or long-wavelength regions of the dislocation photoluminescence spectrum, respectively.

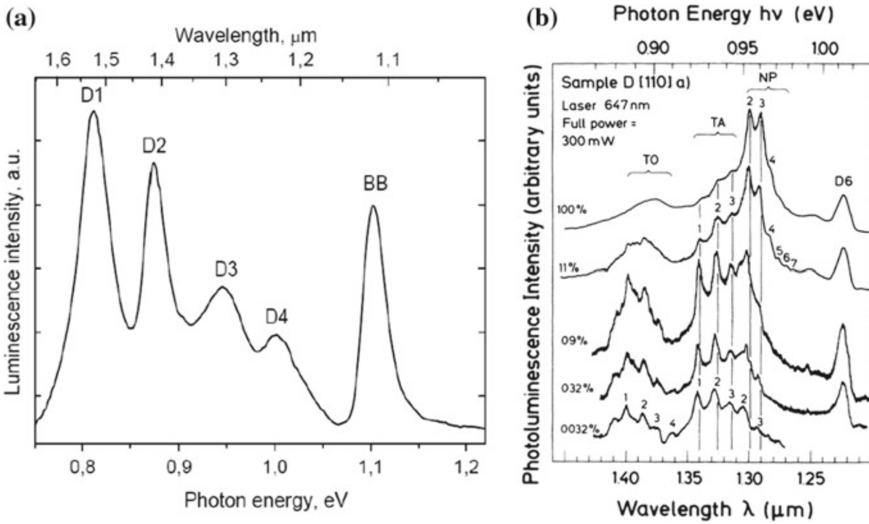

Fig. 21.4 **a** Four main lines of dislocation-related luminescence in Si [10], and **b** excitation dependence of a DRL spectrum as typical of all of the two-stage deformed Si samples. Reproduced with permission from [50]. Copyright (1986) by the American Physical Society

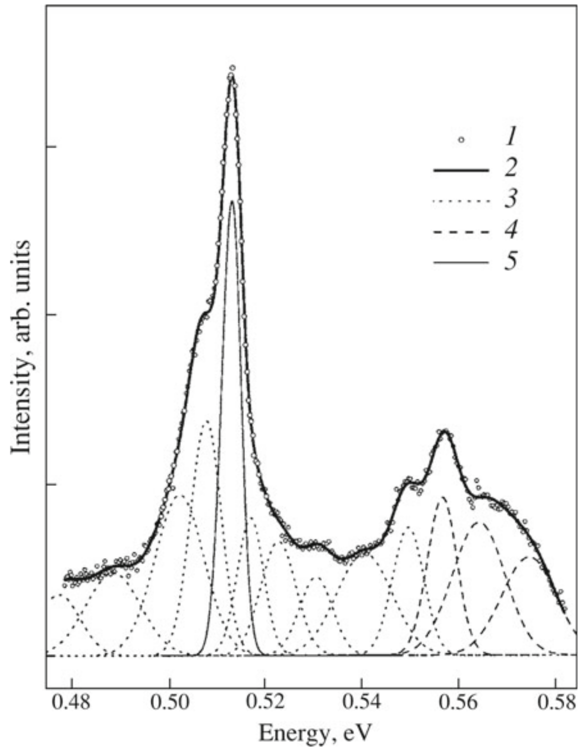

Fig. 21.5 Photoluminescence spectrum of Ge sample with the dislocation density $ND = 3 \times 10^5$ cm^{-2}: (1) experimental points, (2) total approximating curve, (3) Gaussian lines at energies $En \leq 0.55$ eV, (4) Gaussian lines at energies $Em > 0.55$ eV, and (5) the $d8$ line, from [44]

Though different empirical expression [50, 55] to describe the position of the spectral components and different shapes of the dislocation potential were considered [56, 57] a consensus about the DRL mechanism was established as the recombination of excitons bound to the shallow deformation related electronic states 90° partial dislocation. The localization energy of exciton E_l defined as the difference between the band gap energy and DRL exciton band was found of the order 100 meV for both Ge and Si in accordance with the sum of the shallow hole and electron states of dislocation [8, 58] but the exciton binding energy was as small as few meV that was ascribed to lowering of effective mass due to 1D character of the electronic system. The impact of the deformation potential of closely spaced 30° partial dislocation was considered as a small perturbation that varies the energy of the mentioned states being a function of the distance between the partials (or SF width) that can take only discrete values. SF itself was assumed neither has own electronic states, nor exhibit any impact on dislocation-related electronic states.

21.4 Dislocation Related Luminescence in ZB Semiconductors

DRL was also found in many monocrystalline ZB lattice II-VI compound semiconductors. The most detailed information about that was obtained for ZnSe [59]. First report about that was published by Dean [60] who found an unusually narrow line labelled as Y in a defect-rich material. In the following it was established that during the growth of ZnSe layers on (001) GaAs substrates by molecular beam epitaxy (MBE) Se(g)-type misfit dislocations first nucleate in pseudomorphic films of high quality above some critical thickness. The individual segments of the Se(g) misfit dislocation appears to be the only local emission centers responsible for Y-line luminescence.

In the insert of Fig. 21.6a the panchromatic CL map of ZnSe/GaAs (100) for a 165 nm epitaxial layer is displayed showing bright contrasts at Se(g) misfit dislocations. The CL contrasts lines are exactly in the [1–10] direction, which corresponds to the Se(g) subsystem misfit defect configuration. The CL emission is found to be dominantly along the [1–10] Se(g) misfit dislocations. The segments of the misfit segments are therefore the active radiative recombination centers. The panchromatic CL signal of misfit segments was found to exceed the matrix CL emission intensity by almost one order of magnitude.

The low energy spectrum displayed in Fig. 21.6a corresponds to Y luminescence line and its first LO phonon replica originating from the segments of Se(g) dislocation.

In the Y luminescence spectrum in Fig. 21.6a besides the main peak at 2.612 eV a number of weaker additional peaks can be resolved at both high and low energy sides. The fine structure of the Y line appears to be of a serial nature as it is shown in Fig. 21.6b [61]. The Y luminescence peak series has been explained by a model based on the assumption of 60° Se(g) dislocation segments to be dissociated into

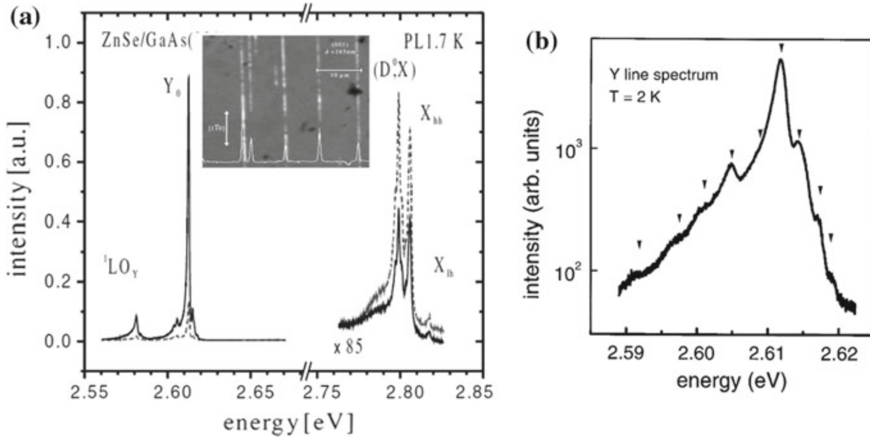

Fig. 21.6 **a** ZnSe/GaAs (001) polarization-dependent PL spectrum. In the insert the panchromatic SEM-CL map (10 kV, 10 K) exhibit bright CL contrasts at Se(g)-type misfit dislocations. The defects are radiative recombination centers as evidenced by the CL intensity profile. Reproduced with permission from [59]. Copyright (2000) IOP Publishing. **b** The fine structure of the Y-line spectrum appears to be of a serial nature. Reproduced with permission from [61]. Copyright (1999) Elsevier

30° and 90° Shockley partials. Nucleation of dissociated Se(g) misfit dislocations has also been verified by TEM examinations of ZnSe/GaAs (001) heterostructures [62]. The CL maps presented in the insert of Fig. 21.6a taken with spectral resolution revealed that the spectral position of Y line varied along the dislocation lines. That was explained to be due to variations of the separation between the partials in the frame of the model described above for DRL in Si and Ge and served an additional confirmation of the validity of this model.

The high energy PL spectrum shown in Fig. 21.6a is dominated by the recombination of the free and donor-bound exciton. The emission from the layer matrix and defect-induced luminescence (Y0) show the polarization dependence: Y luminescence is dominant along the dislocation lines, whereas the free exciton emission is dominant along perpendicular to them directions. Optical polarization parallel to the dislocation line direction is expected by assuming a one dimensional carrier potential [63]. This explained a low value Hyang-Rhys factor ($S = 0.1$) which was previously established to be fingerprint of low-dim system [64]. The high value derived for the defect bound exciton energy of 27 meV [63] confirmed this assumption as well.

It was also found that dissociated screw dislocation segments did not exhibit any luminescence. Thus, the 30° partial dislocations have been excluded as radiative recombination centers. This gave an experimental evidence that the 90° partial dislocation is the most favorable candidate for bound exciton states responsible for Y luminescence.

DRL due to Te(g) but not due to Cd(g) dislocations was found in CdTe [65]. Thus, the dislocations in the corresponding A(g)-subsystems show defect-induced

non-radiative recombination properties. For both B(g) dislocations the shallow levels produced by the deformation potential were assumed to be responsible for DRL optical transitions. By taking into account the strain field only, it is unable to explain the obvious different recombination activity of A(g)- and B(g)-type dislocations in II/VI materials.

ZnSe is a semiconductor that exhibits n-type conductivity only. In opposite to that ZnTe can be only p-type. Two sharp and intense emission bands denoted as Y1 and Y2 with the maxima of 2.185 and 2.150 eV and a weak phonon coupling were investigated in the heteroepitaxial ZnTe layers in [66]. The study of the ZnTe layers grown on different substrates with thicknesses of 0.5–3.2 μm has shown that this luminescence is produced in the interface region that contains a high density of structural defects. TEM [67] revealed an array of Lomer and 60° misfit dislocations at the interface. Also, a small number of stacking faults, limited by partial dislocations, was observed.

The temperature dependence of these band spectral positions revealed the excitonic character of the recombination. Besides, a fine structure of Y1 and Yz bands was observed. In samples with a high intensity of Y1 and Y2 bands it is possible to distinguish LO-phonon replicas, with the values of the Huang-Rhys factor ($S < 0.01$ for Y1 bands and $S = 0.2$ for Y2 bands) that are similar values obtained for DRL in other materials reviewed above.

The luminescence intensity of the Y bands decreases rapidly when the sample warms up and above 80 K these bands disappeared completely. Between 2 and 30 K, the estimated activation energy is about 8 meV, while above 30 K it is about 120 meV. The first activation energy is very close to the binding energy of free exciton in ZnTe (~12 meV), The second one is similar to the localization energy for the hole at acceptor-like centers (~70–100 meV). The first process was ascribed to thermal dissociation of the bound exciton, which liberates the electron, and the second one is due to the activation of the hole bound to a dislocation [66].

Though no direct evidence of dislocation origin of Y band was presented the similarity of the properties of Y band in ZnTe allows us to ascribe this band origin to the dissociated misfit dislocations.

To summarize the properties of DRL band in sphalerite type semiconductors one has to note that the Huang-Rhys factor S is rather small reflecting low-dimensional character of the bound exciton. On the other side the localization energy E_l of DRL band is rather big for all materials (for CdTe ($S = 0.2$, $E = 130$ meV) [65], for ZnSe ($S = 0.2$, $E = 220$ meV) [59] and for ZnTe ($S = <0.1$, $E = 210$ meV for Y1 and $S = 0.2$, $E = 250$ meV for Y2) [66]) and seems to exceed the sum of the energies of shallow electron and hole states due to dislocation deformation potential calculated theoretically [8] by the value that is larger than exciton binding energy being of the order not more than 30 meV.

One of the reason might be that in the above reviewed papers the role of SFs was considered as a separator between the partial dislocations only without taking into account their particular properties in compound semiconductors. That is why we include in this review two recent studies dealt with the SFs in ZnSe and GaAs.

21.5 One Dimensional Defect Formed by Intersection of the (111)-Stacking Fault and Quantum Well in ZnSe

Recently, the results of study of intersections of SF with QW was proposed to consider as the natural 1D system [68]. The samples were grown by molecular beam epitaxy (MBE) on a GaAs:Si (001) substrate covered by an epitaxial GaAs buffer layer of a 0.2 μm thickness. The heterostructures comprised a ZnSe QW with a thickness either 20 or 10 nm, embedded in $Zn_{0.84}Mg_{0.16}S_{0.12}Se_{0.88}$ barriers with thicknesses of 100 nm, and a 2-nm-thick ZnSe cap layer. This design excluded the interpretation of the narrow lines as related to SFs in a bulk material like in [69], because in this case they would emerge near band edge of the barrier material significantly higher in energy than the emission of the ZnSe QW. Besides, the composition of the solid alloy in the barriers was chosen to realize the pseudomorphical growth when the in-plane lattice parameters of GaAs and ZnMgSSe are equal excluding, thus, the formation of misfit dislocations described in the previous Section.

TEM investigations revealed long-extended SFs, with the length of about 10 μm intersecting the sample surface along the direction [1–10] and the short SF pairs which were perpendicular to the extended ones (see Fig. 21.7e). In this way, dislocation-free SF ribbons with the width of 20 or 10 nm and with the length of 100 and 10 μm served as the subject of the micro-photoluminescence investigations carried out at a temperature of 10 K.

New PL peaks were found at the positions of SFs whose were not observed far away from them and were ascribed to the excitons bound to the intersection of the QW and SFs. The lines were red shifted with respect to the free exciton peak by (22–28) meV for the wide QW and by (12–16) meV for the narrower one. The μ-PL spectra for the short SF and QW width of 20 nm are shown in Fig. 21.8 for two polarizations of the excitation. They possess the linewidth <0.5 meV, which suggests the pronounced exciton localization. The polarization degree of narrow lines obtained for the excitation power 10 μW is shown in Fig. 21.8 and exceeds 30%. For long SFs the maximum polarization degree is about 25% and the line was broader that.

As it was pointed above, the SF can be viewed as a two-monolayer-thick inset of a WZ crystal phase embedded in a zinc blende (ZB) structure (see Fig. 21.2). Since the band gap of bulk WZ ZnSe is larger than that of bulk ZB ZnSe, it seems surprising that the exciton can be bound to SFs. However, the WZ phase of ZnSe, being pyroelectric, should possess piezoelectric and spontaneous polarizations, similarly to III-nitride QW structures, which provide an internal electric field along the [111]-type direction. This leads to the offsets eU of the bands at the SF plane, as shown in Fig. 21.7b. Such a band profile was assumed to result in the formation of bound excitons with the electron and hole localized at opposite sides of SF.

DFT calculations presented in [68] in agreement with other recent results [70] predicted that the band gap in the WZ phase is about 100 meV larger than in the ZB phase. The estimated internal electric field in the WZ region was $F = 5 \times 10^5$ V/cm that is comparable to that in GaN [71] giving the value of $eU = 45$ meV and

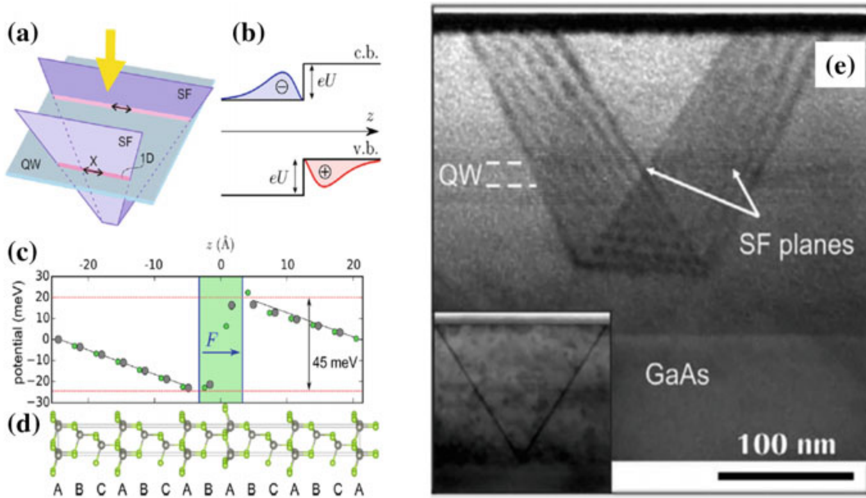

Fig. 21.7 **a** Sketch of SFs planes intersecting a QW. The incident light (yellow arrow) creates bound excitons (X) in this region, which are polarized predominantly along the 1D intersections. **b** Simplified band diagram of a SF in bulk ZnSe and the probability densities of electron and hole in a bound exciton. The band offsets, equal for the conduction and valence bands, are produced by an intrinsic electric field ***F*** within the SF region. **c** The electrostatic potential extracted from the DFT calculation and **d** elementary cell used in this calculation. **e** TEM image of the SFs originating in lower barrier. Reproduced with permission from [68]. Copyright (2018) John Wiley and Sons

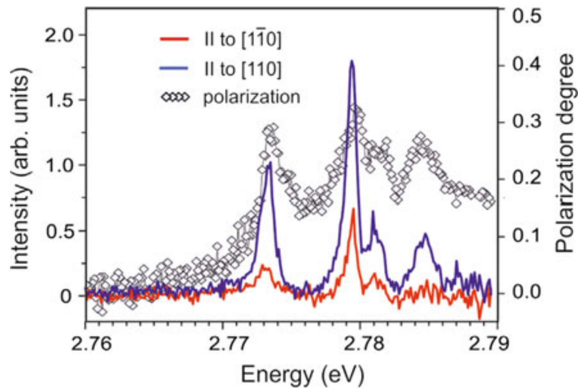

Fig. 21.8 Polarization resolved μ-PL spectra after subtraction of a background related to the main excitonic peak. Reproduced with permission from [68]. Copyright (2018) John Wiley and Sons

calculated exciton binding energy was very close the experimental value for SF of 20 nm width.

The width of the dislocation-free SF ribbon in [68] was 10–20 nm (as defined by the QW width) that is similar to the its width in the core of the dissociated dislocation. The direction of the polarization of the samples with the 1D intersections of the QW and SFs was also the same as for DRL in the ZnSe samples with misfit dislocations. Though the exact band diagram in the vicinity of SF remained unknown the existence

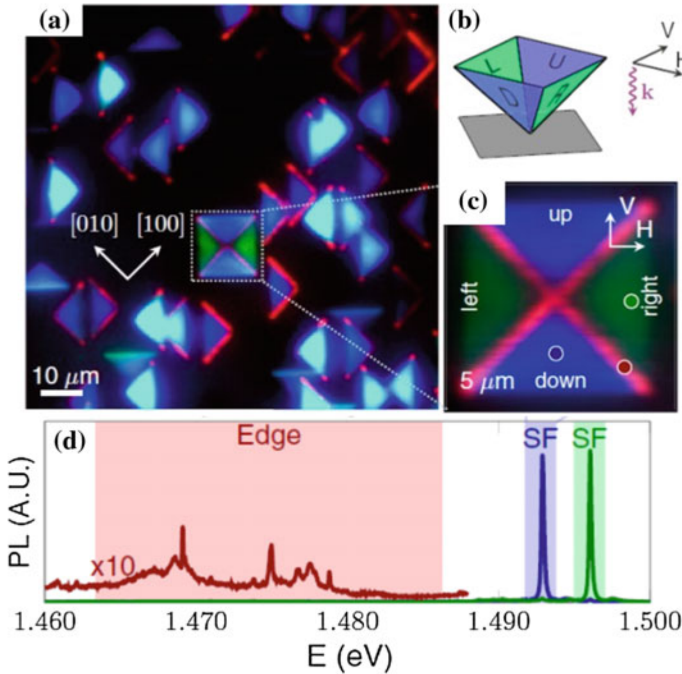

Fig. 21.9 **a** Confocal scan of SF structures. The image is formed by coloring emission in different wavelength bands as red, blue, or green, as depicted in (**d**). Excitation at 1.53 eV, 100 μW, and 1.9 K excite and collect H polarization [see **b**]. **b** Diagram of SF pyramid. The up, down, left, and right SFs are labeled, along with the H and V polarizations. **c** Detail of SF pyramid structure. **d** Low-power PL spectra at colored dots in **c**. Polarizations: blue, excite and collect H; green and red, excite and collect V. Broadband luminescence is observed from the SF edges (red). Reproduced with permission from [67]. Copyright (2016) by the American Physical Society

of additional attraction between the electrons and holes due dipole character of SF charge was demonstrated.

The importance of the spontaneous polarization was recently also demonstrated in GaAs [67] where giant value of the permanent dipole moment of two-dimensional excitons bound to a single SF was found.

SF structures were grown from the substrate epilayer interface during epitaxial growth. They were formed in a 10 μm GaAs layer MBE grown on 100 nm AlAs separated with a 5 nm/5 nm AlAs/GaAs superlattice with a semi-insulating (100) GaAs substrate. Two types of SFs were observed in the layer: a SF pyramid with four possible {111} surfaces and a SF pair defect. They nucleate near the substrate-epilayer interface during epitaxial growth.

Figure 21.9a represents confocal image of SF structures by coloring emission in different wavelength bands as red, blue, or green, as depicted in Fig. 21.9d taken at 1.9 K. Different color of two adjacent faces of a pyramid is due to different spectral line position in two perpendicular light polarization shown in Fig. 21.9b.

Most of the SF defects appear as single triangles, which were identified as a pair of nearby SFs. The binding energy of excitons to a pair of SFs depends varied in the ranges of 20–30 meV being defined by the distance between the SFs. The narrowest full width at half-maximum (FWHM) of the SF PL line in the sample was about 80 μeV at zero magnetic field, that is twice less than the narrowest reported linewidth for a GaAs/AlGaAs quantum well of 130 μeV [72]. This unprecedented homogeneity allowed one to resolve the SF–bound-exciton fine structure that helped to define an absolute value of the exciton dipole moment that was retrieved from the results of the investigations of magneto-Stark effect. The giant dipole moment value was estimated as an elemental charge times 10 nm whereas in conventional excitonic systems, typical electron-hole separations are on the order of several nm.

The existence of such dipole moment of a SF bound exciton was interpreted as a consequence of symmetry breaking and spontaneous polarization similar to that like it was discussed above for SF ribbons in ZnSe. Based on further details of magneto-optic investigations it was speculated that the hole presumably is localized in the SF plane while the electron is weakly bound via the Coulomb interaction. The spontaneous polarization shifts the electron cloud to one side of the SF, resulting in a giant excitonic dipole moment.

As a rough estimate, the interaction energy of two such dipoles will exceed the SF FWHM of 77 μeV when the exciton density is greater than 230 μm^{-2}. Using a wave-function size of approximately 10 nm, the critical density for exciton overlap in the 2D potential is 10,000 μm^{-2}. Therefore, the SF-bound exciton system could show sizable dipole-dipole interactions and may demonstrate coherent phenomena at reasonable exciton densities.

The dislocations bounded SFs which are expected to be of Lomer type in this case are seen in the PL-map in brown. Their DRL spectra denoted as “Edge” in Fig. 21.9e were red shifted with respect to free exciton by 40–60 meV. One can distinguish DRL broad bands with numerous narrow lines. The particular components of the fine spectral were not discussed in [67] but one may assume that the broad bands are due to the variation of distance between dislocations in one SF pyramid like it was discussed for DRL from dissociated dislocations in other material in the previous Sections.

Summarizing the results of this Section one may conclude that SFs in sphalerite type semiconductors possess a property that are unexpected for wider band gap inclusions, being rather quantum barrier than QW but, nevertheless, attractive to exciton making them as a perfect perspective object for further study of many electron system.

This property might be one of the reason why DRL in ZnSe and CdTe could be observed for B(g) but not A(g) dislocations since the SF polarity is the same for both types dislocations but shallow states of deformation potential of the edge dislocations are situated at opposite sides of SF. However, it is early to make definite conclusion and additional, in the first row theoretical, investigation are needed.

21.6 Dislocation-Related Luminescence in Wurtzite Type Semiconductors

21.6.1 Non-polar Lattice SiC

In wurtzite type semiconductors SFs are inclusions with a smaller band gap than the matrix (see Table 21.1). Though the exact band alignment is not known in many cases it is expected that SFs form quantum wells at least for one type of carrier. Dissociation width of dislocations of wurtzite type compounds with partly ionic bonding is usually rather small but for silicon carbide with pure covalent bonding the energy SF is so low that SF width reaches macroscopic sizes that enables to obtain the information about optical properties of SF and bounding partial dislocations by means spectrally resolved optical microscopy.

First of all, one has to mention that despite of a very high hardness of SiC the degradation in the active region was found by forward operating of 4H-SiC PiN diodes. The degradation was caused by spontaneous formation of planar defects identified as basal plane SF bounded by Shockley partial dislocations. Such phenomenon is known a recombination enhanced dislocation glide (REDG) is believed to be responsible for the lateral expansion of SFs. According to the conventional model [73] a part of the electron-hole recombination energy is redirected into nonradiative sites along the dislocation line to aid formation and migration of kinks, thus dramatically reducing the activation barrier for glide. Apart from this strong REDG effect, theoretical models interpret an SF in 4H-SiC as a 2D QW for the conduction band electrons [74]. Since entrapment of electrons in the QWs leads to reduction of the mean electronic energy, a faulted *n*-type crystal is supposed to be more stable than a perfect one. The concept of quasi-Fermi level was suggested [75] to explain the reversible expansion and contraction of SF regions in a degraded 4H-SiC PiN diode, or a virginal 4H-SiC crystal illuminated by above-bandgap laser irradiation. The expansion of SFs is the result of SF energy becoming negative when the quasi-Fermi level for electrons E_{nF} is raised above the SF energy level, thus lowering the total energy of the crystal.

As it was included in the first part of this review there are three types of SFs in wurtzite lattice, single layer (I1 or 1SF), double layer (I2 or 2SF) and E type. Among them only I2 possess glide, However, exclusively 1SF 1SFs expand in presence of the *e*-*h* plasma, whereas 2SF occur in highly *n*-doped material only This issue is beyond of the scope of this review and will not be discussed.

Figure 21.10 a, b represents spectrally selective electroluminescence (EL) imaging in the degraded 4H-SiC diodes taken at 510 nm (2.5 eV) and at 700 nm (1.8 eV). One can see that the first image represents planar-like defects while the second one consists of the lines only. The principal radiative channels are evident from the differential PL spectra plotted in Fig. 21.10c. The stacking faults demonstrate characteristic peaks associated with E_C–0.3 eV and E_C–0.6 eV split-off levels, which are consistent with first principles calculations for 1SF and 2SF related quantum wells [74]. It is interesting to note that partial dislocations bordering 1SF and 2SF type faults exhibit

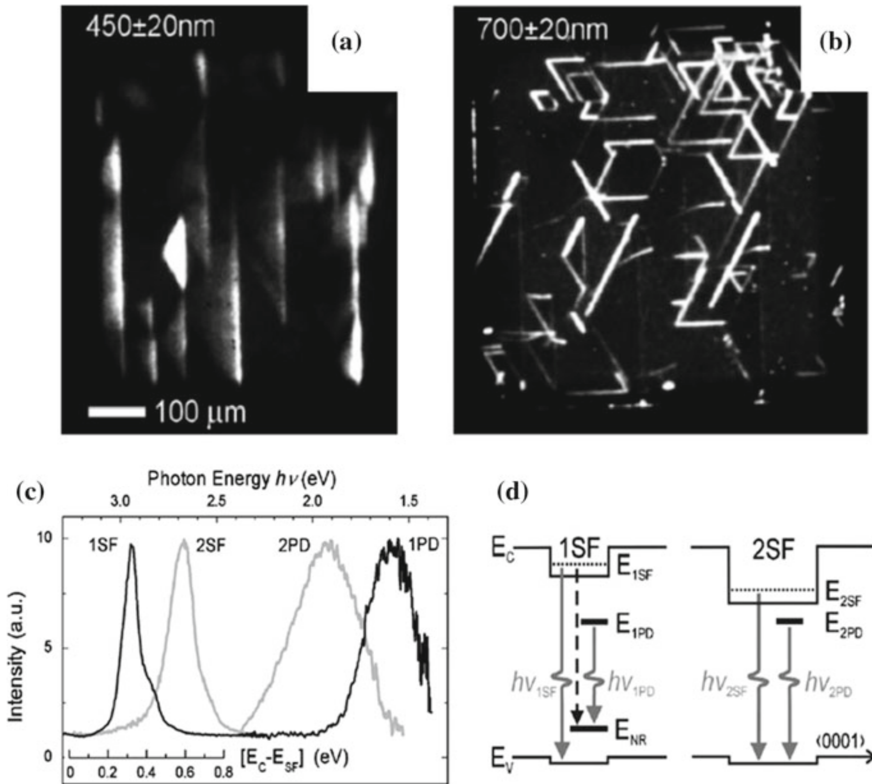

Fig. 21.10 **a**, **b** Spectrally selective plan-view EL imaging in a degraded 4H-SiC p-i-n diode. Defects of various types can be revealed by spectral filtering of EL emission: **a** only the stacking faults can be observed in a wavelength range of 450–620 nm; **b** the bounding partial dislocations and the bright spots of threading dislocations are revealed in the 700–620 nm range; **c** Spectral signatures of normalized PL at 300 K_ of single- _1SF_ and double-layer _2SF_ stacking faults and corresponding bounding partial dislocations, labeled 1PD and 2PD, respectively; **d** Schematic of the bandgap arrangement of 4H-SiC containing 2D quantum-wells formed by 1SF and 2SF in [0001] direction and enclosed by PDs lying along [11–20]. Nonradiative process aiding REDG is marked by a broken arrow; solid arrows indicate radiative transitions. Reproduced with permission from [76]. Copyright (2006) by the American Physical Society

clearly dissimilar spectral signatures corresponding to optical transitions of about 1.6 eV and 1.9 eV, respectively. It was established that luminescence is more intensive for moving Si(*g*) partials edges but a weak emission from the immobile C(*g*) edges also takes place [76]. The luminescence spectra obtained separately from the gliding and the stationary partials appear fairly similar, the latter exhibiting slightly broader high-energy shoulder.

Based on results of luminescence and deep level spectroscopy investigations a collective energy level diagram of recombination activity at 1SF and 2SF type faults was proposed [76] shown in Fig. 21.10d, which accounts for concomitant radiative

and nonradiative processes at mobile Shockley partials as well as for radiative centers along stationary PDs bounding the in-grown SFs. The small valence-band discontinuity and phonon interaction do not notably change the model and are ignored for simplicity. As can be seen in the diagram, the characteristic PL of the PDs bounding 1SF and 2SF type faults then correspond to, respectively, optical transitions from the radiative center directly to the valence band ($h\nu_{2PD} = E_R$ ~ 1.9 eV) and from E_R to the hole-trap E_T introduced by the Si(g) partial ($h\nu_{1PD} = E_R - E_T$ ~ 1.6 eV). In contrast to electrically active and therefore highly mobile Si(g) partials, no midgap levels are introduced by the partials bounding the in-grown 2SFs, resulting both in blue shifted optical signature (towards 1.9 eV) 1234 and absence of REDG effect.

The origin of DRL of the partials in SiC in not established firmly so far. Recent investigation of DRL polarization dependence revealed some unexpected results [77]. In this work the monochromatic PL images were acquired through band-pass filters passing light of 1.64 eV for 30° -Si(g) and 6° PDs, light of 1.34 eV for 30° C(g) PDs, and light of 2.95 eV for SSFs.

It was found that the polarization of the PL from the for 30° -Si(g) and 6° PDs was distinctly polarized perpendicularly to the dislocation lines. This opposite to the DRL polarization in all other semiconductors reviewed above where it was parallel to dislocation lines. The only model that predicted non-parallel dislocation polarization was reported in [78]. It considers the anisotropic effective mass of holes and concluded that the polarization must be parallel to their Burgers vector, in disagreement with the polarization direction in the present results. It was suggested in [77] that the luminescence originates from some dislocation centers of intrinsic nature binding carriers with an anisotropic wave function.

The PL from for 30° C(g) PDs was not polarized and not uniform along the dislocation line but was interrupted at places on the dislocation lines. One might explain these two facts by assuming either that the luminescence originates from impurities inhomogenously distributed along dislocation lines which are centers of radiative or non-radiative recombination.

21.6.2 Dislocation-Related Luminescence in Wurtzite Polar Lattice Compounds

DRL in polar wurtzite compounds was found and investigated in CdS and CdSe [79–86] as well as in GaN [87–93]. DRL in these materials arose from the freshly introduced basal screw dislocations (frequently called as a-screw dislocations) as opposite to cubic lattice semiconductors where 60° dislocations were the sources of DRL. Beside the listed materials, recently luminescence related to some extended defect was reported for ZnO [94] which characterized by a low localization energy of about 40 meV, narrow line and extremely low Huang-Rhys factor indicated about strong confinement of electron-hole pairs. However, the type of the responsible dis-

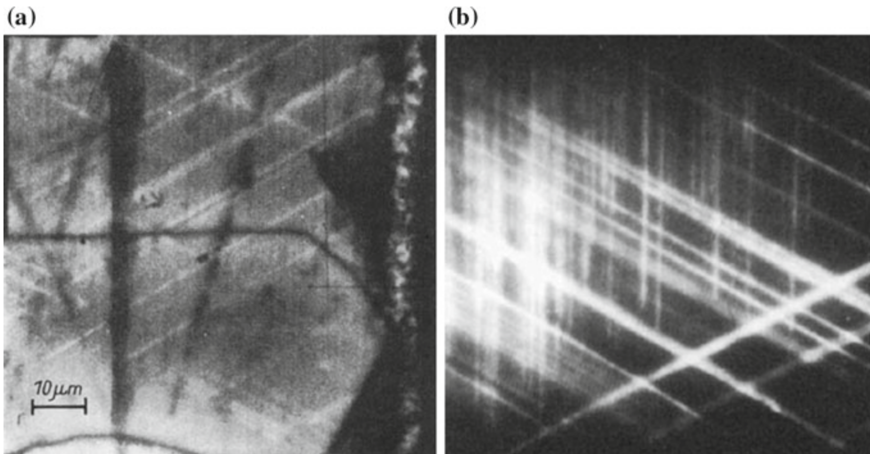

Fig. 21.11 **a** SEM-CL micrograph (20 kV, 80 K) [79] and **b** optical micrograph from (0001) surface of deformed CdS sample. The bright stripe shaped contrasts indicating a local increase of integral luminescence intensity stretched out in {1–210} directions. T = 77 K. Reproduced with permission from [83]. Copyright (1991) John Wiley and Sons

location, if any, remained unknown and the results of this study will not be discussed here.

The most extended information was obtained for CdS. The first reports about DRL in CdS was published in [79, 95] before DRL in silicon was discovered. The luminous dislocations could be viewed both by SEM CL and in optical microscope as they presented in Fig. 21.11a and 21.11b respectively.

The directions of the straight lumibous lines were {1-210} that unambiguously indentify them as a-screw dislocations. The luminous line were observed in plastically deformed crystal by uniaxial compression [80, 83, 84, 86], by identation [82, 83, 96] and by scratching [82] at room temperature. It was established that a-screw dislocations exhibited the same luminescent properties in both basal and prismatic glide systems and DRL could be observed below 150 K. Moreover, the motion of dislocation was observed even at liquid helium temperature [83, 84]. TEM study [97] revealed that the dislocations in basal glide system of all types are dissociated into partials with the SF ribbons of several nm and can glide in the dissociated state.

DRL spectrum taken from the area with multiple dislocations revealed a band of spectral lines shifted with respect to band gap by 100–120 meV. DRL fine structure consists of two doublet components which, in turn, split in two other under application of uniaxial elastic deformation as it is seen in Fig. 21.12. Detailed investigation of the evolution of the spectral positions of the doublet components allowed one to define the symmetry of the radiation center as C_s. It was concluded that the single screw dislocation has two kinds of such centers twofold degenerated in {1-210} plane which are situated immediately in the core of the dislocations. So, each of the splitting line

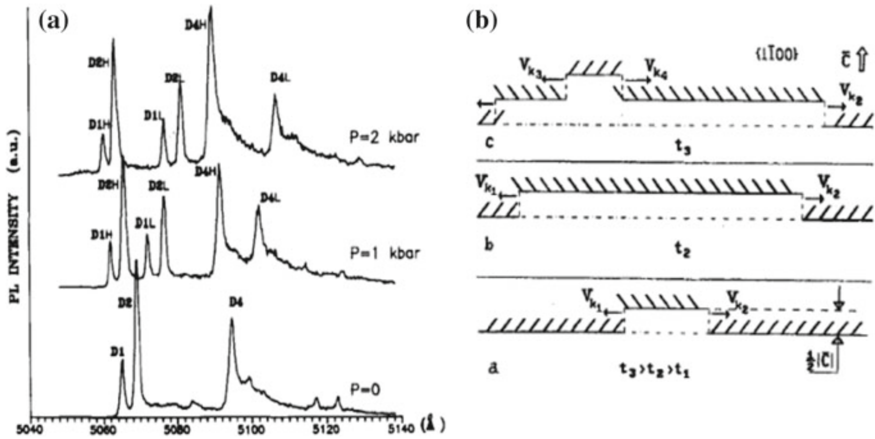

Fig. 21.12 **a** Photoluminescence spectra at T = 6 K showing the dislocation luminescence in CdS sample taken at different uniaxial pressure under an angle of 600 to the screw dislocations. **b** Schematic diagram of the space- and time-nonstationarity of the dislocation domains caused by the distribution alteration of one-dimensionally ordered Cs, centers in the screw dislocation core. Reproduced with permission from [85]. Copyright (1993) AIP publishing

components corresponds strictly to a certain type of screw dislocation—right or left with respect to their expansion direction.

In addition as it was noted in [84, 85] the moving screw dislocations observed in polarized light, with the electric-field vector E of the light forming an angle of 45–65° with the C axis, appeared to have a domain structure. As a result, screw dislocations that are continuous in unpolarized light appear in polarized light as separate scintillating segments or domains whose number can both increase and decrease with time in a discontinuous manner. When the vector E deviates from the direction indicated, the nonstationary nature of the DE becomes less noticeable. It appears that the domain structure depends on the temperature, the loading, and heavily on the optical excitation level. Also, it has been found that when a dislocation domain is quenched in one polarization it rises in the other, and vice versa. Thus, the DRL polarization directions in CdS was non-parallel to the dislocation lines and, so, different from DRL in cubic lattice materials.

The model of twofold oriented radiation center in the dislocation core proposed in [85] is schematically shown in Fig. 21.12b. According to this model, the nonstationary domain structure of screw dislocations is directly related to the reorientation of one-dimensionally ordered C, centers. Therefore, the glide of a screw dislocation segment along the C axis because of the formation and subsequent expansion of double kinks will be inevitably followed by the dislocation center reorientation. This model explained qualitatively the increase in domain scintillation frequency with increasing deformation temperature and applied stress. The strong effect of the optical excitation level on the nonstationary character of the domain structure may well be due to the stimulating action of laser illumination on the nucleation of

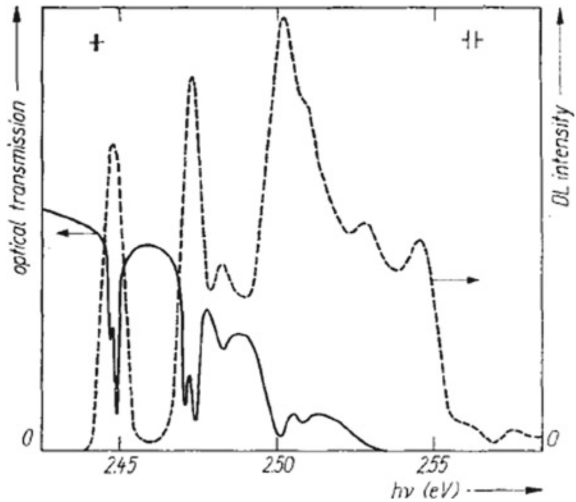

Fig. 21.13 Optical transmission spectrum (full line) and excitation spectrum of dislocation luminescence (hv = 2.45 eV, dashed line) at T = 4.2 K in plastically deformed CdS. Reproduced with permission from [80]. Copyright (1988) John Wiley and Sons

kinks from nonradiative processes on the dislocations similar to conventional REDG model.

One should underline that the model implicitly assumes that the screw dislocation has a perfect core structure as it glides in [0001] whereas according to the mentioned TEM data most of the observed moving dislocations are dissociated though in some cases of coalesce of partials into perfect core were reported as well [97]. The motion of the screw dislocation in C direction was also reported in [82, 98] where the dislocations in the near-surface region introduced by indentation or scratching of the basal surface disappeared completely after sample exposure at room temperature.

The mechanism for DRL of screw dislocation in CdS was discussed in [44] based on the coincidence of their energetic peak positions in absorption and excitation and luminescence spectra (Fig. 21.13). These facts together with a small FWHM of the optical dislocation bands lead to the conclusion about more probable the model of excitons bound to the metastable point defect complexes generated in plastically deformed samples.

Finally, screw dislocations were shown to accompany with an electrical level in the forbidden gap with binding energy of about 100 meV [98]. The level exhibits metastable behavior having an enthalpy for electron emission of 0.4 eV and a capture barrier of about 0.3 eV. One may not exclude that such center plays a role in DRL due the closeness of its binding energy to the DRL localization energy but no evidence for that is available up to now.

GaN crystals are grown mostly heteroexpitaxially for LED and HEMT production. This results in a high, more than 10^6 cm^{-2}, density of grown-in dislocations. That is why a few attempts to establish correlation between recombination properties of GaN and the presence of the dislocations have been made.

There are several reports of the investigations on a macroscale, mostly with PL, of the samples with various dislocation density. Shreter et al. [99] reports on correlation

between the intensity of the luminescence bands around 3.4 eV at 11 K in MOCVD GaN on SiC with the density of threading dislocations. Two other luminescence bands Y_7 (3.2 eV) and Y_4 (3.35 eV) found in thin MBE grown GaN films and were related to edge-type threading dislocations in [100]. However, they were not registered in other samples with the same threading edge-type dislocations density [101]. This might be explained with an extrinsic nature of Y_4 and Y_7 responsible luminescence centers, i.e. with either some native point defect or impurity atoms segregated on edge-type threading dislocation [100]. The structure of dislocations introduced by bulk plastic deformation at 950 °C of HVPE GaN and their PL spectra were investigated by Yonenaga et al. [102]. It was reported that the dislocation glide destroyed yellow luminescence band with appearance of the new 1.79, 1.92, and 2.40 eV bands. Based on the TEM results and on the impact of the post-annealing on PL spectra the authors ascribed observed luminescent properties evolution to segregation of V_{Ga}-O_N complexes at prismatic edge dislocations. However, due to an unavoidably high initially dislocation density in as-grown materials the conclusions about the origin of dislocation-related luminescence in GaN made from the data on macro scale are arguable.

There are only limited number of the published works with direct observations of luminous dislocations.

CL study in TEM reveals a band at 3.29 eV of grown-in partial dislocations terminated basal SF [103]. Albrecht et al. [88] investigated the foils prepared from indented at 370 °C of (000–1) GaN using the same technique as in [103] and found an another broad band at 2.9 eV due to a-type 60° dislocations in basal plane while a-screw dislocations were reported to recombine non-radiatively. The 2.9 eV band was observed with a background of another intense broad luminescence band that hindered to give clear interpretation of its origin.

Recently, iron doped semi-insulating (SI) GaN with freshly introduced perfect a-screw dislocations was found to exhibit intense narrow luminescence line with the peak energy of about 3.35 eV at low temperatures [87]. The main DRL peak accompanied with the phonon replica (Fig. 21.14a).

Temperature and power dependences of dislocation-related luminescence (DRL) spectrum allowed to ascribe DRL to exciton bound at the dislocations. The intensity of the DRL decreased with the temperature with an activation energy of 16 meV and the peak could not be registered above 100 K. Huang-Rhys factor derived from the relation of integrated intensity of the zero-phonon peak and its first phonon replica gave extremely small value of $S = 0.017$. TEM study revealed perfect character of a-dislocation cores. Polarization-dependent measurements showed DRL polarization along the dislocation line direction. The intensity ratio of DRL peak measured for polarization along and perpendicular to the dislocation line was 8:1.

The obtained DRL localization energy of 140 meV is surprisingly large for perfect core dislocations owing only shear strain around it. The matter is that Γ point s-like conduction band minimum must be not sensitive to such kind of strains, and only quantum confined levels for the holes can be formed by the dislocations which are not deeper than 0.1 eV according simple single band model [8, 105]. In more sophisticated calculations Albrecht et al. [87] and later Belabbas et al. [104] demonstrated

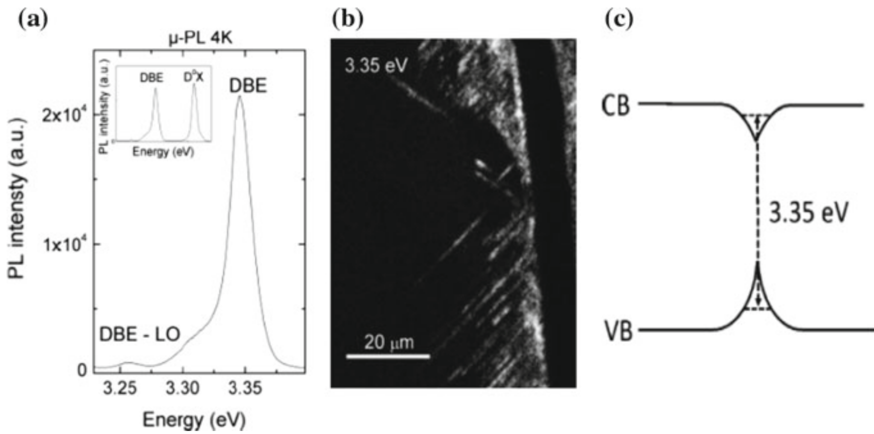

Fig. 21.14 **a** PL spectrum of a single a-type screw dislocation from a micro-photoluminescence map in semi-insulating GaN (0001) taken at 4 K. The inset shows the donor-bound exciton (D0X) and the dislocation-bound exciton in comparison. **b** Monochromatic cathodoluminescence map taken at an energy of 3.346 eV. Straight bright lines correspond to a-type screw dislocations aligned along <1–120>. Reproduced with permission from [87]. Copyright (2014) by the American Physical Society. **c** Band diagram at screw dislocation with DRL optical transition

the existence of the conduction band bending at screw dislocations in GaN arose as a result of the addition of the higher conduction bands into consideration. However, the energy of the electron quantum confined level was not reported, though the knowledge of its value is crucial to explain the observed exciton localization energy which is a sum electron and hole level energies like it is depicted in the diagram of DRL optical transition in Fig. 21.14c.

An intense luminescence band with a lower than in [87] energy of 3.15–3.18 eV at 70 K related to a-screw dislocations was observed independently by two other groups [89, 106]. The results of the investigation [89, 106] were obtained on dislocations introduced by nano- or micro-indentation or scratching of specially undoped low-ohmic GaN. Besides, it was found in [92] that DRL band 3.15–3.18 eV is frequently accompanied with the band of 3.33 eV at 70 K the position of which is rather close to DRL in semi-insulating GaN [87] but as it was shown in [92] has different origin.

Figure 21.15a represents panchromatic CL map near the scratch on c-plane reproduced from [92]. Small dashed line squares with numbers 1, 2, 3 mark the positions of the electron beam where the CL-spectra of Fig. 21.15b were acquired in spot mode. The spectrum in the point 1 (solid line in Fig. 21.15b) corresponds to well-known spectrum of as-grown GaN crystals with the most intense line of free exciton (FE) at 3.46–3.47 eV, and two other lines at 3.27 and 3.4 eV investigated in more details in [101].

Careful examination of the map recognizes two kinds of bright CL-contrasts clearly visible on the dark background. The first one is the straight stripes stretched-out in {12–10} directions being as long as up to 50 μm making a-screw dislocations

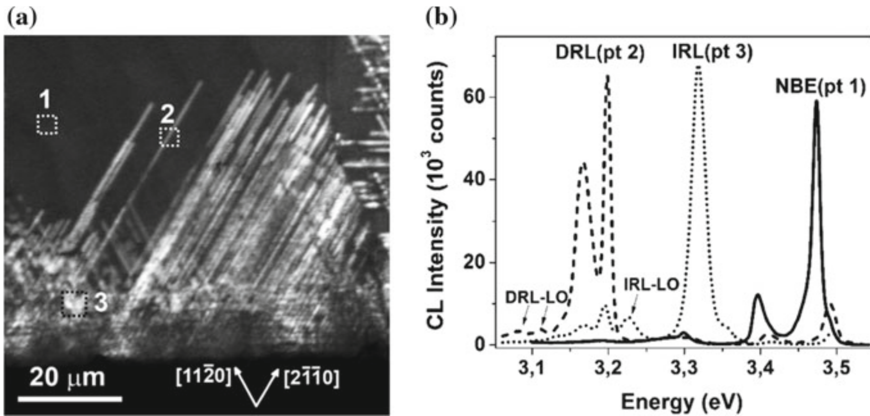

Fig. 21.15 **a** CL panchromatic image near the scratch (black bottom stripe) on c-plane of GaN; **b** CL spectra taken at the positions of electron beam marked in Fig. 21.15a as 1, 2, 3. T = 70 K. Reproduced with permission from [92]. Copyright John Wiley and Sons (2017)

as the most possible candidate for their origin. On the spectrum of the bright stripes (position 2 in Fig. 21.15a), shown as dashed line in Fig. 21.15b, an additional doublet of intense narrow lines at 3.1–3.2 eV is clearly visible. The spectral features are evidently a property of a-screw dislocations, i.e. DRL.

There are also two satellites red-shifted by 90 meV to the main doublet, the shift value that concise well with LO-phonon energy in GaN. A rough estimation of the intensity ratio of the phonon replicas to the ones of the main components from the data in Fig. 21.15b gives a rather low the Huang-Rhys factor $S < 0.1$. Full width at half maximum (FWHM) of main DRL components was reported to be close to that for FE (about 10–16 meV at 70 K). The temperature and strain variation of spectral position of DRL and FE coincided also very well [107]. It was also pointed out that the integrated intensity of DRL lines was significantly higher than FE's intensity far away from the scratch under the same excitation conditions [92]. All listed features gave arguments to interpret DRL in that spectral region as exciton bound at a-screw dislocations [93] whose spectral position in low-ohmic n-GaN differs from that for semi-insulating GaN reported in [87] due to different a-screw dislocation core structure in the materials of different conductivity level. CL spectra acquired from the regions near the indentation prick were identical for indentation of either basal or prismatic planes. This fact allowed one to conclude [93] that DRL spectrum belong only to straight a-screw dislocations gliding in both prismatic and basal plane, while prismatic edge dislocations as well as all non-straight, curvilinear dislocations in basal planes act as non-radiative recombination centers.

The second bright contrast type in Fig. 21.15a is bright spots that are mostly concentrated not so far away from the scratch. Dotted line in Fig. 21.15b is the spectrum taken in the electron beam position 3 of a bright spot in highly dislocated region.

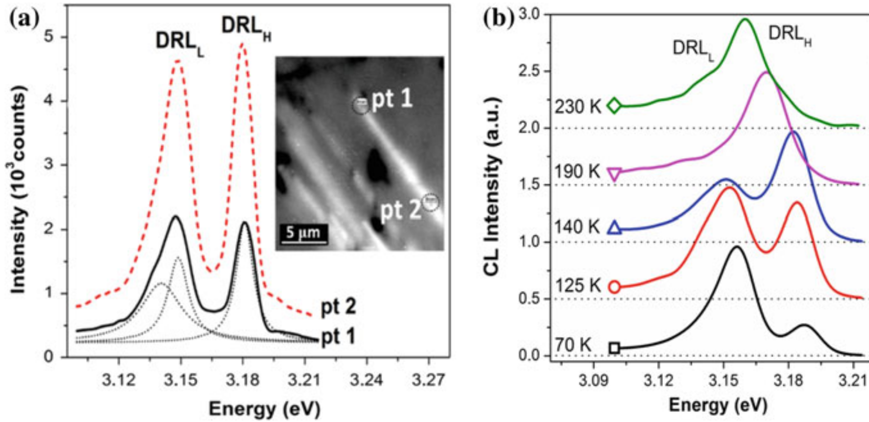

Fig. 21.16 **a** DRL spectra in two points of an alone a-screw dislocation marked as pt 1 and pt 2 in CL-map in the insert. Black dot lines are results of fitting DRL spectrum in pt 1 by Lorentz functions. T = 70 K, E_b = 8 keV, I_b = 500 pA; **b** Temperature variation of DRL spectral doublet shape. Reproduced with permission from [93]. Copyright AIP publishing (2018)

The new spectral feature at this point is a strong luminescence band IRL (intersection-related luminescence) with the peak energy of 3.3 eV while the intensity of DRL is reduced drastically indicating that the IRL band stems on the cost of DRL band. The appearance of IRL band was found in [92] also at the intersections of the screw dislocations intentionally created by two closely spaced indentations. To explain this fact it was proposed that the dislocation nodes formed by the reactions between intersecting screw dislocations are responsible for the IRL.

It was reported [93] that presence of the DRL doublet structure did not depend on dislocation density and was the property of individual a-screw dislocation. Figure 21.16a demonstrates two DRL spectra acquired in two points pt 1 and pt 2 of a single dislocation line shown on CL map in the insert of Fig. 21.16a as well as the approximation of the doublet components with Lorenz function (dotted lines). The high-energy component DRL_H seems to be a single line while the low energy one DRL_L possesses an unresolved fine structure.

The doublet components exhibit also the different behavior of their intensity and shape upon temperature changes as it is demonstrated in Fig. 21.16b. The DRL_H line does not change significantly its intensity and shape up to 190 K. The full width at half maximum (FWHM) of DRL_H in the range 70–190 K changes from about 16 to 25 meV coinciding well with the absolute change of FWHM of FE line. The intensity DRL_L line at temperatures below 120 K exceeds well that of DRL_H but their ratio rapidly decrease with the temperature. Besides, DRL_L quickly broadens with temperature increase and above 170 K the DRL_L line could be recognized only as a little hump on the low energy tail of DRL_H line (Fig. 21.16b). The doublet structure disappears completely at the room temperature turning into a single DRL band with FWHM of about 90 meV broadened from low energy side.

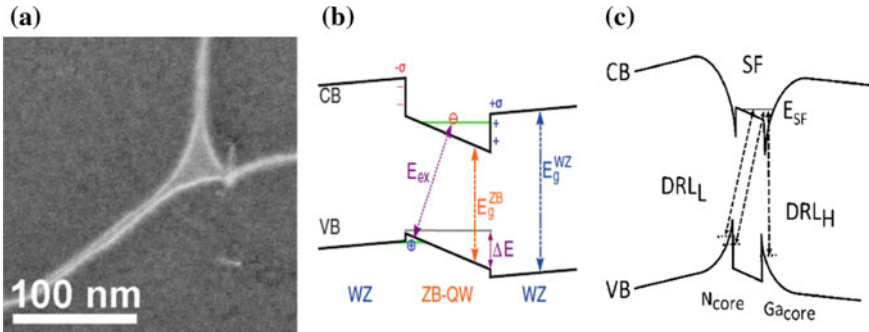

Fig. 21.17 **a** STEM image of a dissociated screw dislocation forming an extended node (Reproduced with permission from [93] Copyright AIP publishing (2018)); **b** Schematic band profile of a stacking fault band alignment in GaN. The polarization induced sheet charges σ leading to the QCSE and the resulting change in the transition energy Eex by ΔE are indicated; **c** Sketch of band diagram of the dissociated screw dislocation showing DRL transitions between energy level of SF ribbon and two 30° partial dislocations including both deformation and Coulomb potentials of partials

The investigations of the evolution of DRL spectrum and dislocation structure after high temperature treatment [91] revealed significant influence of the annealing on dislocation arrangement, while main DRL spectral features measured at the room and lower temperatures remained unchanged. The straight luminous dislocations increased their length from about 40 to more than 120 μm simultaneously with dislocation density decrease close to the scratch after short treatments at 500–750 K.

The core structure of luminous freshly introduced a-screw dislocations was investigated by TEM and STEM [93]. It was found that the dislocation cores were dissociated into two partials bounding stacking fault ribbon. The SF ribbon width was about 5 nm, which varied a little for different dislocations and also along the dislocation line. TEM investigations revealed also the formation of extended dislocation nodes. In Fig. 21.17a STEM HAADF image of dissociated screw dislocations with a typical extended node is reproduced from [93]. One can note that the typical diameter of the extended node of about 15–20 nm exceeds well the width of the dissociation of straight dislocation segments.

The fact that a-screw dislocations are dissociated allows to explain why straight dislocations introduced by scratching of basal surface were stable upon high temperature annealing. The reason for that must be impossibility of the motion of the dislocation dissociated in the basal (0001) plane perpendicular to that plane.

SF ribbon in the core of dissociated dislocation can be considered as an inclusion of GaN sphalerite phase, which has the band gap of 3.27 eV, and therefore forms a quantum well (QW) inside the wurtzite matrix [39, 108] with the conduction band offset of 0.27 eV. Luminescent line of double-layered SF I2, located in the core of extended a-screw dislocation, is red-shifted towards FE energy by about 0.15 eV. Its energy position was reported to vary in the range 3.32–3.36 eV (see recent review [40]). The spectral position of I2 SF line coincides precisely with the position of

observed IRL-band of a-screw dislocations intersections, which can be explained by large area of the extended nodes that exceeds well the exciton Bohr radius [101].

The red shift of SF luminescence with respect expected from theoretically predicted in a simple model [39] was proposed [40] to be due to the spontaneous polarization of wurtzite phase that is absent in sphalerite one that changes the shape of QW potential from rectangular to triangle one as it is depicted in the diagram of Fig. 21.17b. This idea was transferred to explain the DRL properties in low-ohmic GaN.

In the cores of the two 30° partials, bounding the double layered I2 SF ribbon, are predominantly either Ga or N atoms. Being charged Ga^+ and N^- cores of the partials induce an additional electric field [104]. This additional electric field superpose with the electric field of spontaneous polarization [40], which leads to the shift of the energy levels of the Ga^+ and N^--terminated partials with respect to each other. In Fig. 21.17c the band diagram in the scope of a model, which takes into account electric field of partials, spontaneous polarization, and deformation potential, is plotted. For Ga^+/N^--terminated partials the deformation and the Coulomb potentials are both attractive for electrons in the conduction band (CB) and for holes in the valence band (VB) respectively. Together with the QW of SF, these attractive potentials form a deeper quantum confined level for electrons in CB (shown in Fig. 21.17c as E_{SF}) that results in net negative total charge of the dislocation and in the appearance of a saddle point of the sum potential [109]. Because Coulomb potential of Ga^+ and N^- is repulsive for the holes and electrons respectively, the total potential for charge carriers remain attractive only in a close vicinity of the corresponding dislocation core.

The exciton Bohr radius in the bulk GaN crystal is about 3 nm [101], which is comparable with the width of the SF ribbon. In this way, the overlap of electron and hole wave functions is sufficient to form a quasi-1D electronic system along the SF ribbon and two kinds of well distinguished optical transitions in the core of the dissociated dislocations are depicted in the diagram Fig. 21.17c. They are the direct transition between the states of the same partial (DRL_H) and the indirect transition between electron state of Ga^+ and hole state of N^- partials (DRL_L).

A strong localization of closely spaced electron and hole wave functions for the direct exciton explains the thermal stability of DRL_H line caused by a high value of exciton binding energy of 1D system [110].

The indirect exciton possesses a weaker overlapping of electron and hole wave functions, and accordingly, a lower binding energy. On the other side, the density of the holes attracted by negatively charged N-partial line exceeds that at positively charged Ga-partial. As the results, DRL_L transition probability can become larger than one of DRL_H at sufficient low temperatures but becomes less with temperature increase. Previously such kind of behavior (quantum confined Stark effect) was observed for QW structures in external electric field as well as for SFs in GaN in spontaneous polarization induced electric field [110].

21.7 Summary

In this report we summarized the data about dislocation-related and stacking fault-related luminescence in semiconductors with diamond-like, zink-blend and wurtzite lattice structure. Both types of defect were found to possess intrinsic luminescence bands with the specific for given material properties. Despite of extensive investigation of these phenomena an unambiguous understanding of all details of the radiative recombination processes is still lacking.

Important point that previously has not been considered so far is the existence intrinsic luminescence of quantum barriers formed by SFs in sphalerite crystals caused by its dipole moment due to spontaneous polarization in thin wurtzite layer that was shown to play an important role even when SF-ribbon is as narrow as dislocation dissociation width. This fact might help to understand existing issues and stimulate further experimental and theoretical investigations, especially the last ones.

Among the reviewed dislocation-related luminescent bands the only two of them has been reported to survive at room temperature that makes them as candidate for the usage in applications. These are D1 luminescence in Si (0.8 eV) and DRL in GaN (3.2 eV).

The origin of D1 is still under the debate. It is not known whether D1 is an intrinsic or extrinsic property of dislocations in Si that makes impossible to estimate a value of theoretically reachable efficiency of LEDs.

DRL intensity in GaN was shown to exceed well that of band-band radiation and an intrinsic character is undoubtful. Exact theoretical investigations and the development of the technology to prepare electroluminescent devices based on DRL GaN are needed to make final conclusions about its applicability in practice.

References

1. S. Ruvimov, P. Werner, K. Scheerschmidt, U. Gösele, J. Heydenreich, U. Richter, N. N. Ledentsov, M. Grundmann, D. Bimberg, V.M. Ustinov, A.Y. Egorov, P.S. Kop'ev, Z.I. Alferov, Phys. Rev. B **51**, 14766 (1995)
2. M.V. Rakhlin, K.G. Belyaev, G.V. Klimko, I.S. Mukhin, D.A. Kirilenko, T.V. Shubina, S.V. Ivanov, A.A. Toropov, Sci. Rep. **8** (2018)
3. Q. Zhu, J.D. Ganière, Z.B. He, K.F. Karlsson, M. Byszewski, E. Pelucchi, A. Rudra, E. Kapon, Phys. Rev. B **82** (2010)
4. T. Someya, H. Akiyama, H. Sakaki, Phys. Rev. Lett. **76**, 2965 (1996)
5. V.G. Dubrovskii, G.E. Cirlin, I.P. Soshnikov, A.A. Tonkikh, N.V. Sibirev, Y.B. Samsonenko, V.M. Ustinov, Phys. Rev. B **71** (2005)
6. P.B. Hirsch, J. Phys. Colloq. **40**, C6 (1979)
7. M. Heggie, R. Jones, Philos. Mag. Part B **48**, 365 (1983)
8. J.-L. Farvacque, P. François, Phys. Status Solidi B **223**, 635 (2001)
9. M. Reiche, M. Kittler, H. Übensee, M. Krause, E. Pippel, Jpn. J. Appl. Phys. **53**, 04EC03 (2014)
10. N.A. Drozdov, A.A. Patrin, V.D. Tkachev, JETP Lett. **23** (1976)

11. O.S. Medvedev, O.F. Vyvenko, A.S. Bondarenko, Semiconductors **49**, 1181 (2015)
12. P. Yu, M. Cardona, *Fundamentals of Semiconductors: Physics and Materials Properties*, 4th edn. (Springer, Berlin Heidelberg, 2010)
13. I. Yonenaga, Eng. Fract. Mech. **147**, 468 (2015)
14. J.P. Hirth, J. Lothe, *Theory of Dislocations* (Krieger Pub. Co., 1982)
15. J. Hornstra, J. Phys. Chem. Solids **5**, 129 (1958)
16. D.J.H. Cockayne, I.L.F. Ray, M.J. Whelan, Philos. Mag. J. Theor. Exp. Appl. Phys. **20**, 1265 (1969)
17. I.L.F. Ray, D.J.H. Cockayne, Proc. R. Soc. Lond. A **325**, 543 (1971)
18. A.M. Gómez, P.B. Hirsch, Philos. Mag. J. Theor. Exp. Appl. Phys. **36**, 169 (1977)
19. F.C. Frank, J.F. Nicholas, Lond. Edinb. Dublin Philos. Mag. J. Sci. **44**, 1213 (1953)
20. F. Bechstedt, U. Grossner, J. Furthmüller, Phys. Rev. B **62**, 8003 (2000)
21. A. García, M.L. Cohen, Phys. Rev. B **47**, 4215 (1993)
22. J. Lähnemann, Phys. Rev. B **86** (2012)
23. Y.A. Osipiyan, I.S. Smirnova, Phys. Status Solidi B **30**, 19 (1968)
24. Y.A. Osipyan, I.S. Smirnova, J. Phys. Chem. Solids **32**, 1521 (1971)
25. R. Jones, A. Umerski, P. Sitch, M.I. Heggie, S. Öberg, Phys. Status Solidi A **138**, 369 (1993)
26. S.P. Beckman, X. Xu, P. Specht, E.R. Weber, C. Kisielowski, D.C. Chrzan, J. Phys. Condens. Matter **14**, 12673 (2002)
27. R. Landauer, Phys. Rev. **94**, 1386 (1954)
28. S. Winter, Phys. Status Solidi B **79**, 637 (1977)
29. C. Elbaum, Phys. Rev. Lett. **32**, 376 (1974)
30. V.V. Kveder, R. Labusch, Y.A. Ossipyan, Phys. Status Solidi A **92**, 293 (n.d.)
31. R. Labusch, J. Phys. III **7**, 1411 (1997)
32. I. Yonenaga, Y. Ohno, T. Yao, K. Edagawa, J. Cryst. Growth **403**, 72 (2014)
33. V. Kveder, M. Badylevich, E. Steinman, A. Izotov, M. Seibt, W. Schroter, Appl. Phys. Lett. **84**, 2106 (2004)
34. A. Loshachenko, A. Bondarenko, O. Vyvenko, O. Kononchuk, Phys. Status Solidi C **10**, 36 (2013)
35. U.M. Gösele, H. Stenzel, M. Reiche, T. Martini, H. Steinkirchner, Q.-Y. Tong, Solid State Phenom. **47–48**, 33 (1996)
36. S. Marklund, Phys. Status Solidi B **108**, 97 (1981)
37. N. Lehto, Phys. Rev. B **55**, 15601 (1997)
38. C.-Y. Yeh, S.-H. Wei, A. Zunger, Phys. Rev. B **50**, 2715 (1994)
39. Y.T. Rebane, Y.G. Shreter, M. Albrecht, Phys. Status Solidi A **164**, 141 (1997)
40. J. Lähnemann, U. Jahn, O. Brandt, T. Flissikowski, P. Dogan, H.T. Grahn, J. Phys. Appl. Phys. **47**, 423001 (2014)
41. R. Newman, Phys. Rev. **105**, 1715 (1957)
42. S. Shevchenko, A.N. Tereshchenko, Solid State Phenom. **131–133**, 583 (2007)
43. D.B. Holt, B.G. Yacobi, *Extended Defects in Semiconductors* (Cambridge University Press, 2007)
44. S.A. Shevchenko, A.N. Tereshchenko, Phys. Solid State **49**, 28 (2007)
45. V.V. Kveder, M. Kittler, Mater. Sci. Forum **590**, 29 (2008)
46. M. Reiche, M. Kittler, Crystals **6**, 74 (2016)
47. V. Higgs, E.C. Lightowlers, S. Tajbakhsh, P.J. Wright, Appl. Phys. Lett. **61**, 1087 (1992)
48. T. Sekiguchi, S. Ito, A. Kanai, Mater. Sci. Eng. B **91–92**, 244 (2002)
49. T. Mchedlidze, O. Kononchuk, T. Arguirov, M. Trushin, M. Reiche, M. Kittler, Solid State Phenom. **156–158**, 567 (2009)
50. R. Sauer, C. Kisielowski-Kemmerich, H. Alexander, Phys. Rev. Lett. **57**, 1472 (1986)
51. Y.S. Lelikov, Y.T. Rebane, S. Ruvimov, A.A. Sitnikova, D.V. Tarhin, Y.G. Shreter, Phys. Status Solidi B **172**, 53 (1992)
52. V. Higgs, M. Goulding, A. Brinklow, P. Kightley, Appl. Phys. Lett. **60**, 1369 (1992)
53. X. Yu, W. Seifert, O.F. Vyvenko, M. Kittler, T. Wilhelm, M. Reiche, Appl. Phys. Lett. **93**, 2 (2008)

54. R. Sauer, J. Weber, J. Stolz, E.R. Weber, 13 (n.d.)
55. A.N. Izotov, A.I. Kolyubakin, S.A. Shevchenko, E.A. Steinman, Phys. Status Solidi A **130**, 193 (1992)
56. V.Y. Kravchenko, JETF **80**, 9 (1995)
57. Y.S. Lelikov, Y.T. Rebane, Y.G. Shreter, *Structure of Property Dislocations Semiconductors* (eds. by S.G. Roberts, Holt, P.R. Wilshaw, Bristol, 1989), p. 119
58. J.L. Farvacque, P. Franc, Phys. B Condens. Matter **274**, 995 (1999)
59. U. Hilpert, J. Schreiber, L. Worschech, L. Höring, M. Ramsteiner, W. Ossau, G. Landwehr, J. Phys.: Condens. Matter **12**, 10169 (2000)
60. P.J. Dean, A.D. Pitt, M.S. Skolnick, P.J. Wright, B. Cockayne, J. Cryst. Growth **59**, 301 (1982)
61. L. Worschech, W. Ossau, A. Waag, G. Landwehr, U. Hilpert, J. Schreiber, Y.T. Rebane, Y.G. Shreter, Phys. B **273–4**, 895 (1999)
62. A. Rosenauer, T. Reisinger, F. Franzen, G. Schütz, B. Hahn, K. Wolf, J. Zweck, W. Gebhardt, J. Appl. Phys. **79**, 4124 (1996)
63. Y.G. Shreter, Y.T. Rebane, O.V. Klyavin, P.S. Aplin, C.J. Axon, W.T. Young, J.W. Steeds, J. Cryst. Growth **159**, 883 (1996)
64. D.J. Mowbray, O.P. Kowalski, M.S. Skolnick, M. Hopkinson, J.P.R. David, Superlattices Microstruct. **15**, 313 (1994)
65. J. Schreiber, L. Höring, H. Uniewski, S. Hildebrandt, H.S. Leipner, Phys. Status Solidi A **171**, 89 (1999)
66. A. Naumov, K. Wolf, T. Reisinger, H. Stanzl, W. Gebhardt, J. Appl. Phys. **73**, 2581 (1993)
67. T. Karin, X. Linpeng, M.M. Glazov, M.V. Durnev, E.L. Ivchenko, S. Harvey, A.K. Rai, A. Ludwig, A.D. Wieck, K.-M.C. Fu, Phys. Rev. B **94** (2016)
68. D.S. Smirnov, K.G. Belyaev, D.A. Kirilenko, M.O. Nestoklon, M.V. Rakhlin, A.A. Toropov, I.V. Sedova, S.V. Sorokin, S.V. Ivanov, B. Gil, T.V. Shubina, Phys. Status Solidi RRL—Rapid Res. Lett. **12**, 1700410 (2018)
69. P. Corfdir, P. Lefebvre, J. Appl. Phys. **112**, 053512 (2012)
70. F. Boutaiba, A. Belabbes, M. Ferhat, F. Bechstedt, Phys. Rev. B **89**, 245308 (2014)
71. J. Lähnemann, O. Brandt, U. Jahn, C. Pfüller, C. Roder, P. Dogan, F. Grosse, A. Belabbes, F. Bechstedt, A. Trampert, L. Geelhaar, Phys. Rev. B **86**, 081302 (2012)
72. S.V. Poltavtsev, Y.P. Efimov, Y.K. Dolgikh, S.A. Eliseev, V.V. Petrov, V.V. Ovsyankin, Solid State Commun. **199**, 47 (2014)
73. K. Maeda, S. Takeuchi, Jpn. J. Appl. Phys. **20**, L165 (1981)
74. H. Iwata, U. Lindefelt, S. Öberg, P.R. Briddon, Phys. Rev. B **65**, 033203 (2001)
75. A. Galeckas, J. Linnros, P. Pirouz, Phys. Rev. Lett. **96**, 1 (2006)
76. A. Galeckas, A. Hallén, S. Majdi, J. Linnros, P. Pirouz, Phys. Rev. B **74**, 233203 (2006)
77. H. Rii, T. Hidekazu, T. Michio, M.I. Kohei, M. Koji, Appl. Phys. Express **6**, 011301 (2013)
78. M.A. Razumova, V.N. Khotyaintsev, Phys. Status Solidi B **174**, 165 (n.d.)
79. O. Brümmer, J. Schreiber, Ann. Phys. **483**, 105 (1972)
80. N.I. Tarbaev, J. Schreiber, G.A. Shepelskii, Phys. Status Solidi A **110**, 97 (1988)
81. A. Hoffmann, J. Christen, J. Gutowski, Adv. Mater. Opt. Electron. **1**, 25 (1992)
82. O. Vyvenko, A. Zozime, Mater. Sci. Eng., B **24**, 105 (1994)
83. V.D. Negrii, Y.A. Osipyan, N.V. Lomak, Phys. Status Solidi A **126**, 49 (1991)
84. V.D. Negrii, J. Cryst. Growth **117**, 672 (1992)
85. V.D. Negrii, J. Appl. Phys. **74**, 7008 (1993)
86. N.I. Tarbaev, G.A. Shepel'skii, Semiconductors **32**, 580 (1998)
87. M. Albrecht, L. Lymperakis, J. Neugebauer, Phys. Rev. B **90**, 241201 (2014)
88. M. Albrecht, H.P. Strunk, J.L. Weyher, I. Grzegory, S. Porowski, T. Wosinski, J. Appl. Phys. **92**, 2000 (2002)
89. O.S. Medvedev, O.F. Vyvenko, A.S. Bondarenko, Semiconductors **49**, 1181 (2015)
90. O.S. Medvedev, O.F. Vyvenko, A.S. Bondarenko, V.Y. Mikhailovskii, V.E. Ubyivovk, P. Peretzki, M. Seibt, A.I.P. Conf, Proc. **1748**, 020011 (2016)
91. O. Medvedev, O. Vyvenko, A. Bondarenko, Phys. Status Solidi C **1700111**, 1 (2017)
92. O. Medvedev, O. Vyvenko, Phys. Status Solidi RRL—Rapid Res. Lett. **1700297** (2017)

93. O. Medvedev, O. Vyvenko, E. Ubyivovk, S. Shapenkov, A. Bondarenko, P. Saring, M. Seibt, J. Appl. Phys. **123**, 161427 (2018)
94. M.R. Wagner, G. Callsen, J.S. Reparaz, J.-H. Schulze, R. Kirste, M. Cobet, I.A. Ostapenko, S. Rodt, C. Nenstiel, M. Kaiser, A. Hoffmann, A.V. Rodina, M.R. Phillips, S. Lautenschläger, S. Eisermann, B.K. Meyer, Phys. Rev. B **84**, (2011)
95. O. Brümmer, J. Schreiber, Krist. Tech. **9**, 817 (1974)
96. O.F. Vyvenko, A.A. Istratov, Phys. Solid State **36**, 1794 (1994)
97. D.J.H. Cockayne, A. Hons, J.C.H. Spence, Philos. Mag. A **42**, 773 (1980)
98. A.A. Istratov, O.F. Vyvenko, J. Appl. Phys. **80**, 4400 (1996)
99. Y.G. Shreter, Y.T. Rebane, T.J. Davis, J. Barnard, Darbyshire, M. Steeds, J.W. Perry, Camb. J. Online AU **449**, (1996)
100. M.A. Reshchikov, D. Huang, L. He, H. Morkoç, J. Jasinski, Z. Liliental-Weber, S.S. Park, K.Y. Lee, Phys. B Condens. Matter **367**, 35 (2005)
101. M.A. Reshchikov, H. Morkoç, J. Appl. Phys. **97**, 061301 (2005)
102. I. Yonenaga, H. Making, S. Itoh, T. Goto, T. Yao, J. Electron. Mater. **35**, 717 (2006)
103. R. Liu, A. Bell, F.A. Ponce, C.Q. Chen, J.W. Yang, M.A. Khan, Appl. Phys. Lett. **86**, 021908 (2005)
104. I. Belabbas, J. Chen, M.I. Heggie, C.D. Latham, M.J. Rayson, P.R. Briddon, G. Nouet, Model. Simul. Mater. Sci. Eng. **24**, 075001 (2016)
105. Y.T. Rebane, Phys. Rev. B **48**, 14963 (1993)
106. J. Huang, K. Xu, Y.M. Fan, M.T. Niu, X.H. Zeng, J.F. Wang, H. Yang, Nanoscale Res. Lett. **7**, 150 (2012)
107. O.S. Medvedev, O.F. Vyvenko, A.S. Bondarenko, J. Phys. Conf. Ser. **690**, 012008 (2016)
108. J.R.L. Fernandez, F. Cerdeira, E.A. Meneses, J.A.N.T. Soares, O.C. Noriega, J.R. Leite, D.J. As, U. Köhler, D.G.P. Salazar, D. Schikora, K. Lischka, Microelectron. J. **35**, 73 (2004)
109. M. Trushin, O.F. Vyvenko, Solid State Phenom. **205–206**, 299 (2013)
110. J. Lähnemann, O. Brandt, C. Pfüller, T. Flissikowski, U. Jahn, E. Luna, M. Hanke, M. Knelangen, A. Trampert, H.T. Grahn, Phys. Rev. B **84**, 155303 (2011)